applied sciences

MDPI

Communication

Novel Fault Diagnosis of Bearings and Gearboxes Based on Simultaneous Processing of Spectral Kurtoses

Len Gelman [1,*] and Gabrijel Persin [2]

[1] Department of Engineering and Technology, University of Huddersfield, Huddersfield HD1 3DH, UK
[2] Qualimental Technologies Ltd., London N1C 4AX, UK
* Correspondence: l.gelman@hud.ac.uk

Abstract: Diagnosis of bearings and gears, traditionally uses the envelope (i.e., demodulation) approach. The spectral kurtosis (SK) is a technique used to identify frequency bands for demodulation. These frequency bands are related to the structural resonances, excited by a series of fault-induced impulses. The novel approach for bearing/gear local fault diagnosis is proposed, based on division of bearing/gear vibration signals into specially defined short duration segments and simultaneous processing of SKs of all these segments for damage diagnosis. The SK-filtered vibrations are used for diagnostic feature extraction further subjected to the decision-making process, based on k-means and k-nearest neighbors. The important feature of the proposed approach is robustness to random slippage in bearings. The experimental validation of a bearing inner race local defects (1.2% relative damage size), and simulated gear vibration (15% relative pitting size), shows a very good diagnostic performance on bearing vibrations and gear vibrations to diagnose local faults. Novel diagnostic effectiveness comparison between the proposed technology and wavelet-based technology is performed for diagnosis of local bearing damage.

Keywords: gearbox; bearing; vibrations; diagnosis; spectral kurtosis

Citation: Gelman, L.; Persin, G. Novel Fault Diagnosis of Bearings and Gearboxes Based on Simultaneous Processing of Spectral Kurtoses. *Appl. Sci.* **2022**, *12*, 9970. https://doi.org/10.3390/app12199970

Academic Editor: Alessandro Gasparetto

Received: 11 August 2022
Accepted: 22 September 2022
Published: 4 October 2022

1. Introduction

General wear of bearings and gears often leads to unexpected failures, causing unscheduled maintenance interventions, downtime, and economic losses. In the literature, the vibration-based approaches for bearing and gear diagnosis have been widely studied and a variety of processing techniques is currently available [1–10].

Gearbox diagnostic features measure the impulse responses, introduced to gearbox during operation, when pitted teeth come into meshing contact, or bearing rolling elements pass through the faulty races. Damaged components in contact will excite high-frequency resonances of the structure. Moreover, a series of impulse responses in the vibration signal are modulated by shaft or cage frequencies, which is the key fault signature to be recognized in fault identification and localization.

One of the most commonly used approaches is the demodulation analysis (i.e., envelope analysis), where a vibration signal is band-pass filtered and demodulated [2,3,6–9,11]. The spectrum of the envelope is used to detect characteristic defect frequencies in the low-frequency range. Although useful, this approach presents some disadvantages due to the need for selection of the demodulation frequency band and poor performance under high noise levels [3].

To address the challenge of the demodulation frequency band selection, an adaptive SK technique has been proposed and applied to the diagnosis of bearings [2,12–19] and gears [19–22]. As an extension to the SK approach, the fast kurtogram technique has been proposed to determine the optimal SK resolution parameter and generalize the SK approach to a wider class of non-stationary signals [13,14,23]. Furthermore, the SK technique has been used to design detection filters, such as an optimal denoising (Wiener) filters, to extract

non-stationary component with the highest level of impulsiveness from the background stationary noise [24].

Despite improvements, the above techniques did not address varying nature of bearing and gear signals due to a fault progression, a bearing slippage, and varying transmission path. In these conditions, damage-related frequency bands, estimated by the SK, can become less effective resulting in a poor denoising and a non-effective fault diagnosis.

Therefore, in this study, we propose a novel technology based on simultaneous processing of SKs and the optimal denoising (Wiener) filter to address these challenges in rolling element bearings and gearboxes. The main novelty of the technology is a division of bearing/gear vibration signals into specially defined short duration segments, and simultaneous processing of SKs of multiple segments for damage diagnosis. The short duration of segments is defined as a specific time duration corresponding to the slowest modulating frequency of a component. Segments angular alignment, using the cross correlation, allows tracking of impacts, produced by the same rolling element or tooth.

Low speed fluctuations are compensated by applying the angular resampling procedure [24,25]. The frequency bands, selected by the SK for filtering/demodulation, are adapted for each short duration vibration segment to ensure accurate estimation of frequency bands, filtering of the stationary noise, and extraction of—the SK-filtered signals. The SK-filtered signals are demodulated, and a squared envelope is used as the diagnostic feature.

Another paper novelty is a novel diagnosis effectiveness comparison of the proposed technology and wavelet-based technology for diagnosis of local bearing damage.

The main objectives of this paper are:

- to experimentally validate the proposed technology via a bearing test rig during operation under undamaged and damaged conditions,
- to validate the proposed technology via simulation on simulated gear vibration data under undamaged conditions and 15% pitted surface damage, distributed among all teeth,
- to perform a novel diagnostic effectiveness comparison between the proposed technology and wavelet-based technology for diagnosis of a local bearing damage.

2. The Proposed SK Diagnosis Technology

2.1. The SK and Optimal Denoising Filtering

The spectral kurtosis (SK) is interpreted in [12] as an adaptive technique used to determine the most suitable frequency band for an extraction of the non-stationary component. It extends the statistical measure of the kurtosis to the function of frequency and indicates how the impulsivity in the signal is distributed in its frequency domain. As defined in [12], the spectral kurtosis $K(f)$ of the signal $x(t)$ is the fourth-order spectral moment:

$$K(f) = \frac{\left\langle |X(t,f)|^4 \right\rangle}{\left\langle |X(t,f)|^2 \right\rangle^2} - 2 \quad (1)$$

where $\langle\rangle$ is the time average operator and $X(t,f)$ represents the complex envelope of the signal $x(t)$.

The $X(t,f)$ may be estimated by the short-time Fourier transform (STFT) by moving a relatively short window along the signal. The subtraction of 2 in Equation (1) is used to set $K(f) = 0$ in the case $X(t,f)$ contains only noise.

The SK can be used to design detection filters since it takes large values at those frequencies where impulsivity is dominant and low values where there is noise only [3]. It is shown in [8] that the SK of the sum $y(t) = x(t) + n(t)$ where $x(t)$ is the non-stationary

component and $n(t)$ is the stationary Gaussian noise, can be related to the SK of the non-stationary part $x(t)$ by

$$K_y(f) = \frac{K_x(f)}{[1+\rho(f)]} \tag{2}$$

where $\rho(f) = \frac{S_n(f)}{S_x(f)}$ is the ratio of the power spectral densities of $n(t)$ and $x(t)$, reflecting the noise-to-signal ratio with respect to the frequency.

The signal to noise ratio will be high (i.e., $f \approx 0$) within the resonance bandwidth and low outside, in other words, the $K_y(f) \approx K_x(f)$ within the same bandwidth and $K_y(f) \approx 0$ otherwise [13]. Under these assumptions, the Wiener filter

$$W(f) = \frac{1}{1+\rho(f)} \tag{3}$$

is proportional to the square root of the SK, which offers a possibility for SK to identify the optimal filter $W(f)$ for extraction of transients from stationary components [12,13]:

$$\hat{W}(f) = \sqrt{K_y(f)}\ for\ K_y(f) > s\ 0\ otherwise \tag{4}$$

The SK should be compared to the significance threshold, indicating the values significantly greater than zero. In [7,8] a statistical significance threshold $s = s_\alpha$ is calculated on behalf of the properties of the Gaussian noise. Supposing that the signal is only Gaussian stationary noise, the STFT-based SK has a normal distribution with zero mean and variance $\frac{4}{N}$, where N is the number of averages. A statistical threshold given at level of significance is $s_\alpha = u_{1-\alpha}\frac{2}{\sqrt{N}}$, where $u_{1-\alpha}$ is the percentile of the normal distribution at $1-\alpha$ and all values below this level will have probability of $1-\alpha$ of not being a transient [13].

2.2. The Procedure for Extraction of Diagnostic Feature

Figure 1 shows the steps of the proposed technology, which concludes with extraction of the diagnostic features, used for the final diagnosis purposes.

(a) Angular resampling

Systems operating under fluctuating speed (low level of fluctuation) can inaccurately track shaft instantaneous speed and cause spectral smearing of shaft harmonic frequencies. Sampling vibrations signals at constant angular intervals by using optical encoders can alleviate this problem. This is done by interpolating the space between tachometer pulses to obtain the new sample times.

(b) Segmentation into segments

The novel technology proposes segmentation of the vibration signal into specially selected short segments; segment duration is defined as $\frac{1}{(f_r - FTF)}$ seconds for inner race defect, and $\frac{1}{f_r}$ for gear defects, where f_r is the rotational frequency and FTF the cage fault frequency. Duration of each bearing segment is selected in a way, that faulty area is coming into contact with all N rolling elements, and, thus, producing exactly N impulse responses per segment in case of a defective bearing. In case of gears, a gear segment should cover one shaft revolution when all teeth once come into meshing.

(c) Time synchronous averaging (TSA) of gear vibration signal and removal of gear-mesh components

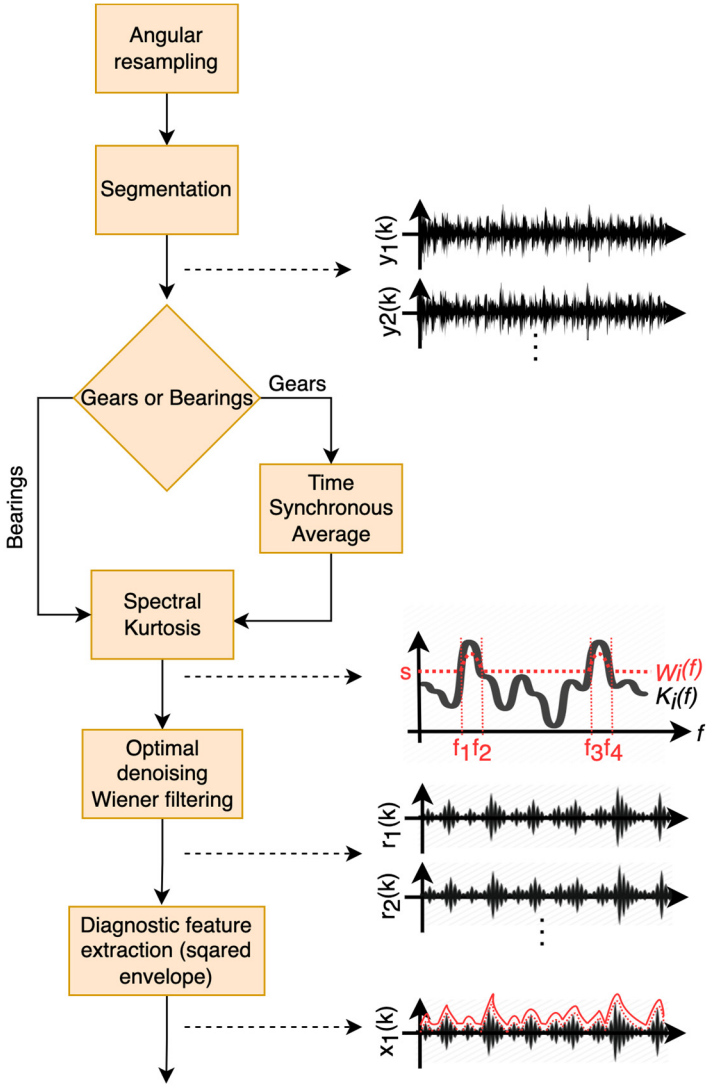

Figure 1. Schematic of the technology for extraction of gearbox/bearing diagnostic features.

Prior to the estimation of the SK and filtering, the raw vibration signal needs to be pre-processed to isolate vibrations of a single component and remove interfering periodic components. Therefore, in case of gears, the SK should be estimated on a gear residual signal, which is obtained by time synchronous averaging and cleaning of periodic gear mesh components.

The time synchronous average (TSA) mt is estimated as the signal average (first order cyclostationary part) on the selected cycle [6] as:

$$m(t) = \frac{1}{N_r} \sum_{k=0}^{N_r-1} x(t - kT_r) \tag{5}$$

where T_r is the period of rotation of the shaft of interest and N_r the number of rotations for the averaging.

The effect of incipient gear tooth fault will be to create a low intensity impact, which may not be visible in the TSA signal itself. Since high intensity mesh harmonics are masking these low intensity impacts, the common practice is to extract these mesh harmonics to form the classical residual signal $r(t)$ [26]. It is shown that the process of removing mesh

harmonics is in fact equivalent to the subtraction of an averaged tooth meshing vibration (the regular signal) from the original TSA signal [27], which reads

$$r(t) = m(t) - \frac{1}{N_t} \sum_{k=0}^{N_t-1} m(t - kT_m) \quad (6)$$

where T_m is the mesh period and N_t the number of teeth of the gear of interest.

(d) Estimation of the spectral kurtosis (SK) and denoising filter

Each signal segment is subjected to the estimation of the SK using Equation (1). The Hamming window is used for STFT estimation, in which the main parameter is the window length. The length should be smaller than the distance between two impulses and larger than the length of a single impulse response [3]. By following these guidelines, the length can be chosen based on BPFI, or F_{gmf}, as they are related to the frequency of the excitation impulses.

In this study, the window length of 1/10 times the duration between consequent impulses is used for processing bearing vibration data, which corresponds to the frequency resolution of 10 times of the bearing characteristic defect frequency. A window size equal to half meshing period is used for estimation of the SK of gear simulated vibrations.

The SK is used to define the Wiener filter by Equation (4). Before filtering, the SK should be compared to so-called the "significance threshold" s that indicates the values of SK greater than the SK produced by the Gaussian noise. It is proposed in [12,13] to use the static statistical significance threshold to filter out all noise components with $1 - \alpha$ probability of not being produced by transients. This way, the filter will produce near-to-zero SK-residuals in the fault-free case, when mostly stationary noise is present, and non-zero SK-residuals in the faulty case.

(e) SK based optimal denoising (Wiener) filtering

Upon estimation of the filter using SK, the filtering is performed in the frequency domain as:

$$Y_i(f) = \hat{W}(f) \cdot X_i(f) \quad (7)$$

where $X_i(f)$ is the Fourier transform of the i-th segment of the raw vibration $x_i(t)$, and $Y_i(f)$ is the Fourier transform of the i-th segment of the SK-filtered signal $y_i(t)$, containing non-stationary impulsive components.

(f) Diagnostic feature extraction SK-filtered squared envelope

The SK- filtered $y_i(t)$ can be considered as an amplitude modulated signal, where the amplitude modulation part, also known as the envelope, reflects the degree of non-stationarity of the fault-induced transients. The envelope can be extracted, using the Hilbert transform [28], and the final diagnostic feature is defined as the squared envelope, reflecting the power of the SK-filtered signal.

(g) Angular alignment of segments by cross correlation to compensate for bearing random slip

To clarify the impulses, which may be affected by random bearing slippage, it is proposed a novel improvement to the squared envelope diagnostic features by aligning the impulses using the cross-correlation approach via the following steps:

1. Initial segment i is considered as a reference to align segment $i + 1$ by maximizing the cross correlation.
2. The mean of aligned segments i and $i + 1$ is taken as a new reference and used to align segment $i + 2$.
3. The mean of aligned segments i, $i + 1$, and $i + 2$ are then used to define the new reference to align segment $i + 3$, and so forward.

The result of the alignment process are straightened lines of impulses allowing to track these impulses, caused by the same ball/roller.

2.3. Diagnosis Effectiveness Estimation

Characterization of technology diagnostic effectiveness is achieved by means of the Fisher criterion (FC) [28], following authors in refs. [4,15,29–36], who also applied the FC to measure a technology diagnostic effectiveness. Thus, we are able to directly compare diagnostic technologies and to evaluate a diagnostic effectiveness, using the FC. The FC is a statistical measure that uses the ratio of the between-class scatter to the within-class scatter to indicate the level of feature separation between damaged and undamaged conditions. For validation of the SK based diagnostic features, the FC is applied as [28]:

$$FC(\theta) = \frac{(\mu_D(\theta) - \mu_{ND}(\theta))^2}{\sigma_D^2(\theta) + \sigma_{ND}^2(\theta)} \quad (8)$$

where μ and σ^2 are, respectively, the mean and variance of the diagnostic features estimated for all segments, D and ND indicate damaged and undamaged conditions, respectively.

The novel decision-making method to rolling element bearings, based on the k-nearest neighbors (kNN) and the majority rule [24,37], is applied in this study. The method considers as training and testing diagnostic features the maximum values of squared envelope from each segment. The approach first creates M one-dimensional clusters of the fault free training data by using the k-means method. After clustering, the calculation of the novelty scores for testing data is done in the following five steps:

- The nearest neighbor distance $dNN1_{ij}$ is calculated for each training data sample xij in the cluster j, where $i = 1, \ldots, N_j$ and $j = 1, \ldots, M$. N_j is the number of samples in cluster j and M is the number of clusters.
- The k maximal NN distances among the N_{j-1} NN distances are used for each cluster and their mean value $D_{1j} = E_{max} dNN_{1ij}$ is calculated.
- Euclid distances between testing data sample y_i and training data samples x_j in cluster j are calculated.
- The averaged kNN distance dNN_2 for cluster j and test data sample is then calculated as the mean value of k minimal NN distances.
- The novelty score of the test data sample for cluster j, NS_{ij}, is calculated as the ratio between distances D_1 and D_1 and average kNN distance dNN_2 as $NS_{ij} = dNN_{2ij} D_{1j}$ and the minimal novelty score for sample y_i is selected.

After decisions are obtained, the total probability of correct diagnosis is used to estimate diagnosis effectiveness.

3. Experimental Technology Validation for Bearing Race Defect

The experimental rig (Figure 2) has a coupled variable speed drive (VSD) motor with 20–60 Hz shaft rotation frequency, adjusting eccentricity of the coupling, and angular or parallel misalignment. The shaft is supported by three pillow block rolling element bearings of the same specification (FK UCP203), where two bearings are fixed (left and middle) and one is a replaceable testing bearing (right).

The specifications of the testing bearing are shown in Table 1, which lists characteristics of bearing geometry and frequencies related to defect of an inner race (BPFI), an outer race (BPFO), a cage (FTF) and a rolling element (BSF) with respect to the frequency of rotation f.

Two sets of experiments were conducted at speed of 3600 rpm, and the resultant radial load of 192 N, which is adjusted by inserting pre-machined shims under the test bearing housing. The first experiment is performed with undamaged bearing, and the second experiment is performed using a bearing with damaged inner race. The inner race defect extended through 0.8 mm of circumferential length and is 0.2 mm deep, with the relative damage size equal to 1.2% of circumference, which indicates an early stage of damage development (Figure 3). The damage level is not critical, it is selected at an early stage of a damage, that is important for multiple industrial applications.

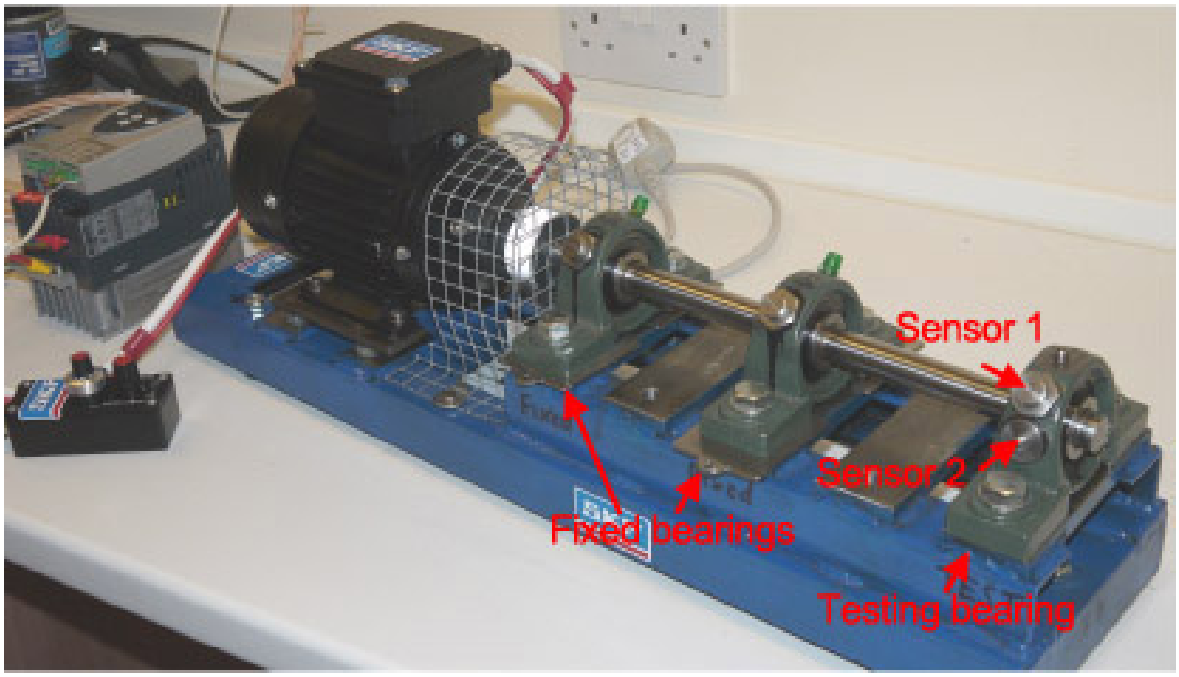

Figure 2. Experimental rig.

Table 1. Test bearing specifications.

Number of Balls n_{re}	8
Bore diameter	17 mm
Outer race diameter	40 mm
Ball diameter	6.75 mm
Ball pass frequency inner race, *BPFI*	4.95*f_r
Ball pass frequency outer race, *BPFO*	3.05*f_r
Ball spin frequency, BSF	1.99*f_r
Fundamental train frequency FTF	0.382*f_r

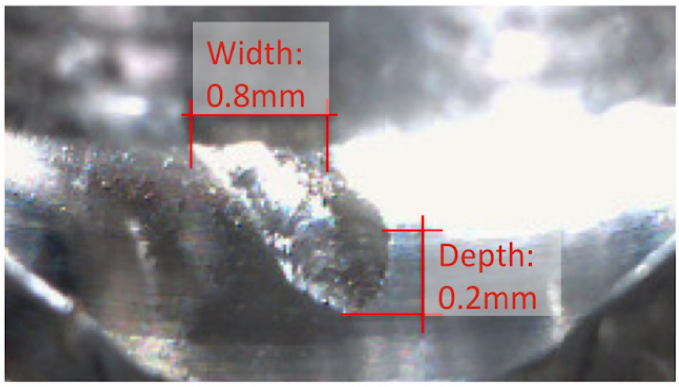

Figure 3. Bearing inner race defect characteristics.

Vibration signals are captured from an accelerometer model KCF AG107M, placed along vertical direction on a test bearing external housing with a specification in Table 2.

Table 2. KCF AG107M accelerometer specification.

Frequency response	1 Hz–5 kHz
Axial sensitivity	5.21 pC/ms^2
Resonance frequency	25 kHz
Max acceleration	80 g
Mass	28 g
Piezo material	PZT-5
Isolation resistance	10 × 109 Ohm
Capacitance	1200 pF
Temperature range	−40 to 150 degC
Shock limit	800 g
Temperature sensitivity	4 mg/degC
Structural strain sensitivity	0.2 mg/micro strain
Magnetic field sensitivity	2 g/T

The output connector featured waterproof sealing. Active antialiasing filter (cut-off frequency = 13.5 kHz) is used before capturing the digitized data. A speed reference signal (1 pulse per shaft revolution) is also captured synchronously. The data sampling is done at 40 kHz to provide a necessary bandwidth for channel recording.

Technology Validation on Inner Race Fault

Bearing vibration signals were resampled into the angular domain using a tachometer signal. The SK is calculated individually for each short vibration segment to identify the excited resonant frequency bands, and the optimal denoising Wiener filter parameters are also adapted individually for each vibration segment. Figure 4 shows the SK vs. frequency for fault free (a) and damaged (b) cases for 340 short segments.

In the fault-free case, the SK remained below 1.5 for all segments and frequency bands (Figure 4a), which suggests the dominant presence of stationary noise of a fault-free bearing. The SK of a damaged bearing shows multiple resonant frequency bands, excited by a fault exceeding amplitude of 12. Figure 4b shows three main resonant frequency bands at central frequencies 5 kHz, 12 kHz and 16 kHz. As can be seem from Figure 4b, the SK has the highest peak amplitude at 12 kHz, which indicates that the structural resonances are dominant within 12 kHz band. The bands at 5 kHz and 16 kHz have slightly lower but comparable amplitude indicating additional resonant behaviour within those bands as well. Given that different realisations excite resonant bands with varying amplitude, this phenomenon could be attributed to the variation in location of the damaged area (the inner race damage is not static; but, rotates with a shaft), which is causing partial smearing of the frequency bands due to two effects: (a) varying fault induced excitations with higher amplitudes, when the damaged area is within the load zone, and with lower amplitude outside; and (b) varying transfer function between the source of the excitation and the sensor with rotating damaged area (unknown transmission path). The varying nature of bearing inner race faults and consequent excitation requires observation of multiple consequent segments over time to capture multiple responses of the bearing, where each response is shown with a different colour in Figure 5. As can be seen in Figure 5, resonances at frequency bands 5 kHz and 12 kHz are excited for three realisatons, while resonances at 16 kHz band were only excited twice out of three times. The amplitude of SK peaks also varies between 12–21, which gives further evidence to varying nature of bearing damage signals.

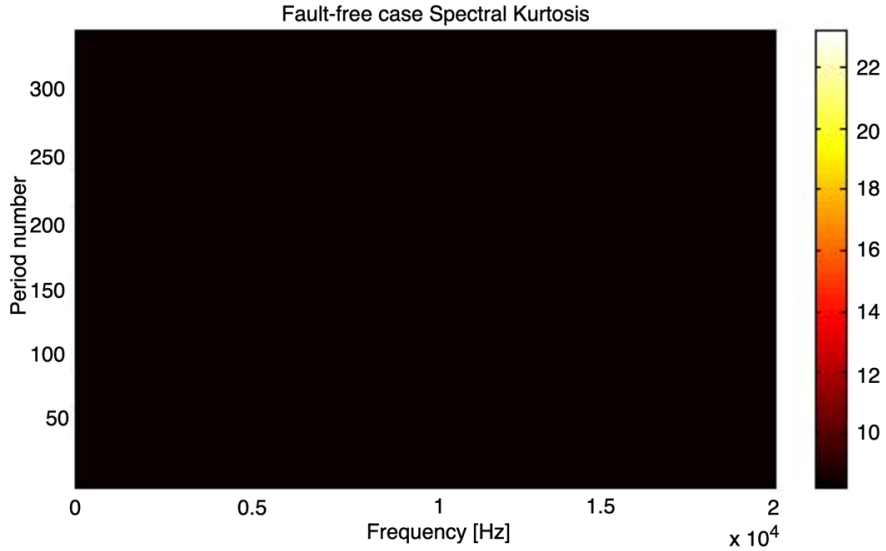

(**a**) Fault-free

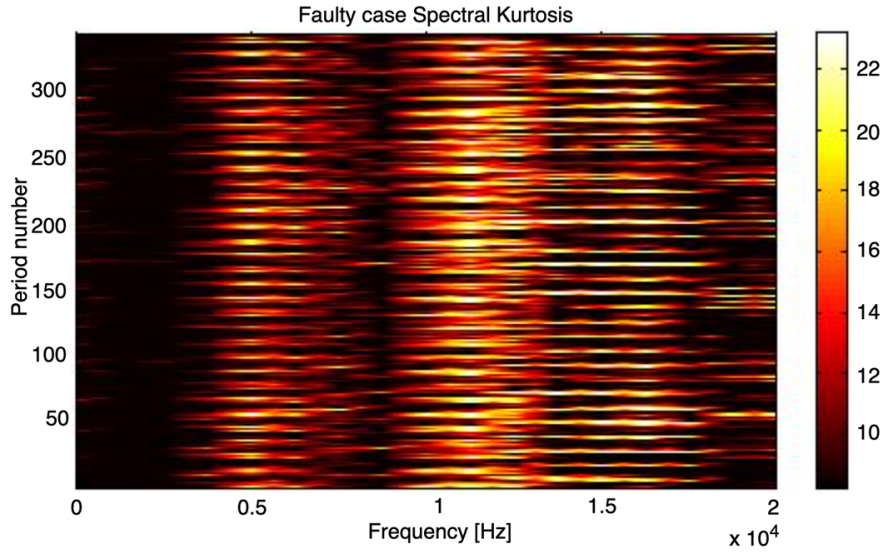

(**b**) Inner race defect

Figure 4. Spectral kurtosis for consequent bearing vibration segments.

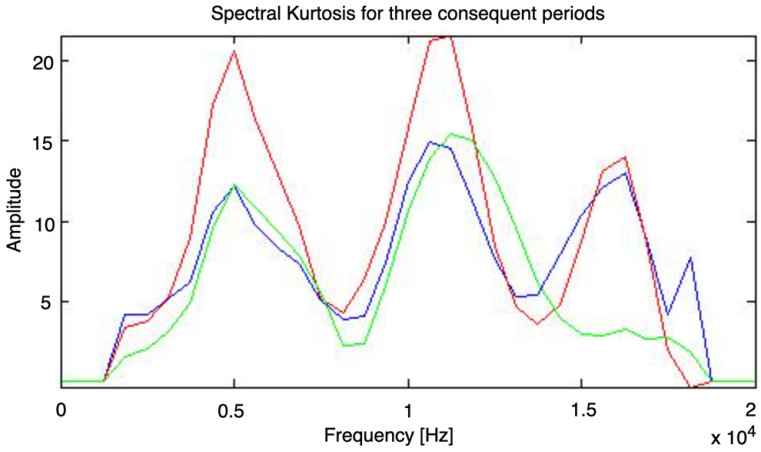

Figure 5. SK for three randomly selected short segments from bearing signal. Three segments are shown with three colors (segment 1 - green, segment 2 - red, segment 3 - blue).

According to Equation (4), the SK is used to design the optimal denoising (Wiener) filter upon being compared to the statistical significance threshold s. The presented results are achieved using 1% statistical significance. The filtering is achieved using Equation (7) in frequency domain, and resulted in removal of the stationary noise, thus, retaining the non-stationary fault-related component—the SK-filtered signal. The diagnostic features for all 340 segments are shown in Figure 6 for fault-free (a) and damaged (b) cases.

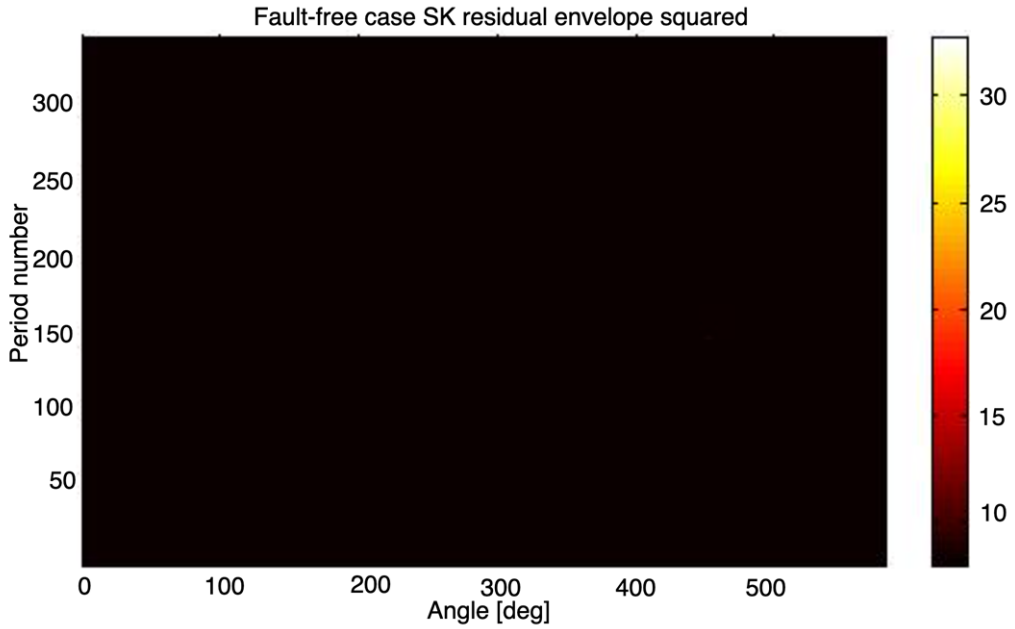

(**a**) Fault-free

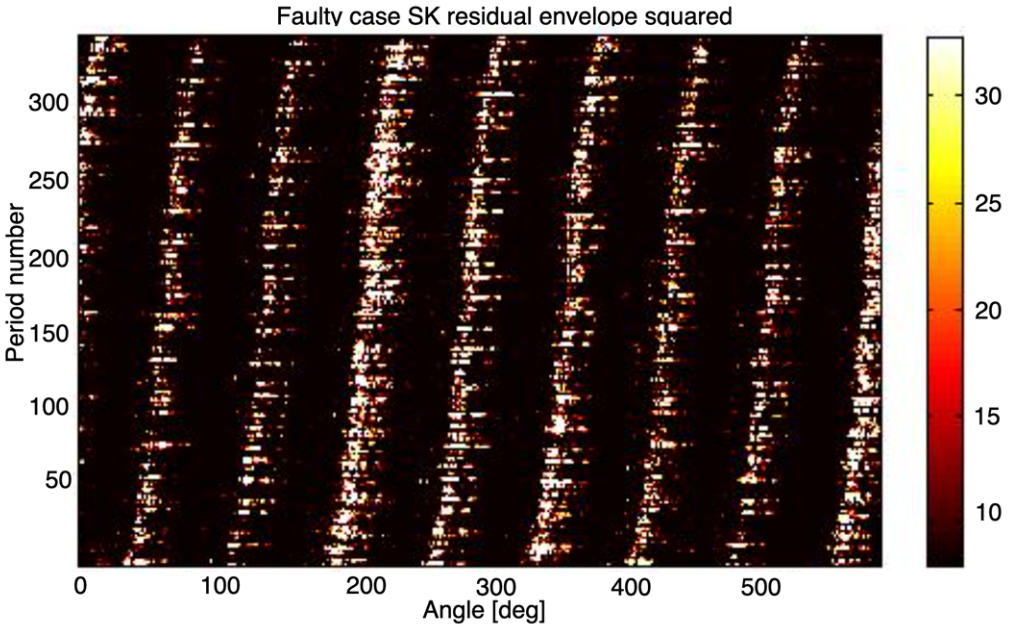

(**b**) Inner race defect

Figure 6. The diagnostic features—squared envelope of the SK-filtered signal.

The feature maps show mainly low amplitude (<10) apart from the high amplitude features in damaged case (b) due to extracted impulsive components. The diagnostic features have high amplitudes at the moment of the impact and low amplitudes between

impacts. According to the specially defined length of each segment, the envelope signals cover exactly 8 impacts, produced by 8 balls of the bearing. Dependency of diagnostic features vs. shaft angle reveals inclined line impact patterns (as expected) rather than straight lines. This phenomenon is due to the presence of the random slippage between the rolling elements and bearing races. Although the impacts are clearly visible, to track impacts, produced by the same rolling element, over prolonged periods of time, additional alignment is performed on all segments, using the novel cross-correlation approach. The alignment, using the novel correlation approach, makes the inclined lines of impacts vertically straight (Figure 7). The main purpose of the alignment is to retain impacts, produced by the same ball/roller within a consistent angular band for improved fault localization.

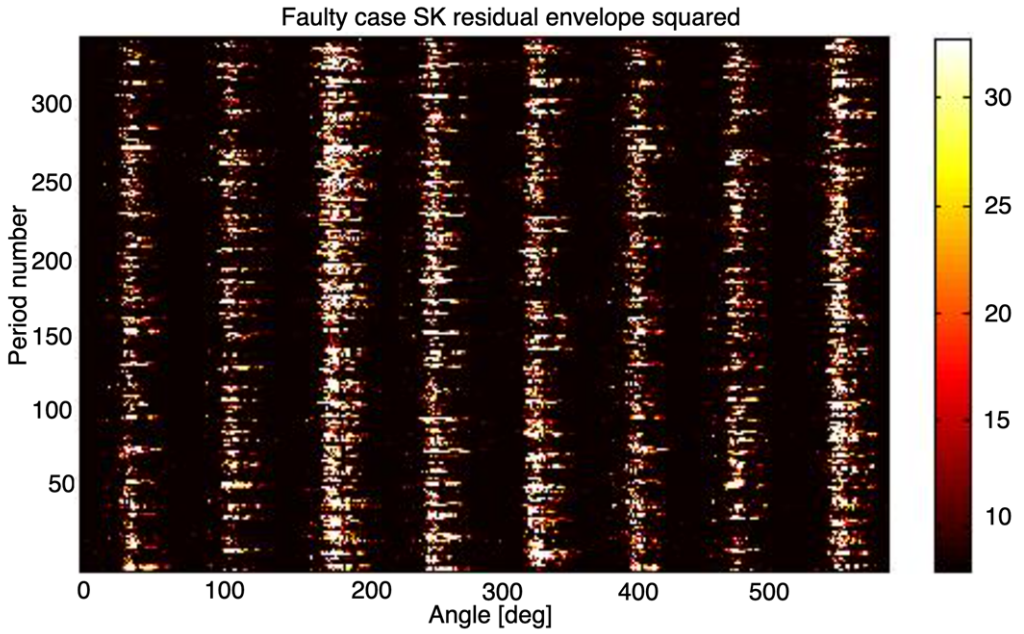

Figure 7. The aligned diagnostic features—squared envelope of the SK filtered signal.

To evaluate the separation between the diagnostic features, extracted under damaged and undamaged conditions, the FC is applied. Figure 8 shows essential values of FC in range [2,4] related to a moment of an impact when a rolling element passed through the damaged inner race area. The FC is calculated based on histograms from damaged and undamaged cases and represents a measure of a separation between them. This means, only a single FC graph is obtained from the entire experiment from both feature histograms for damaged and undamaged conditions. In addition, the FC, shown in Figure 8, is a measure of a separation between the diagnostic feature histograms from inner race defect and undamaged cases, and shows the FC values for a complete cycle, including the time of impact (FC peak values) as well as the time between impacts (FC of low values). The FC values suggest a clear separation between diagnostic features, extracted from damaged and undamaged conditions, which is the main requirement for reliable diagnosis.

The performance of the SK-based diagnostic features defined within this paper is compared to the wavelet-based features obtained from the same vibration signals acquired under the same experimental conditions [5]. The authors have used wavelet transform for frequency band selection as well as filtering for feature extraction and have obtained the FC values close to 1 for all 8 peaks, summarized in Table 3.

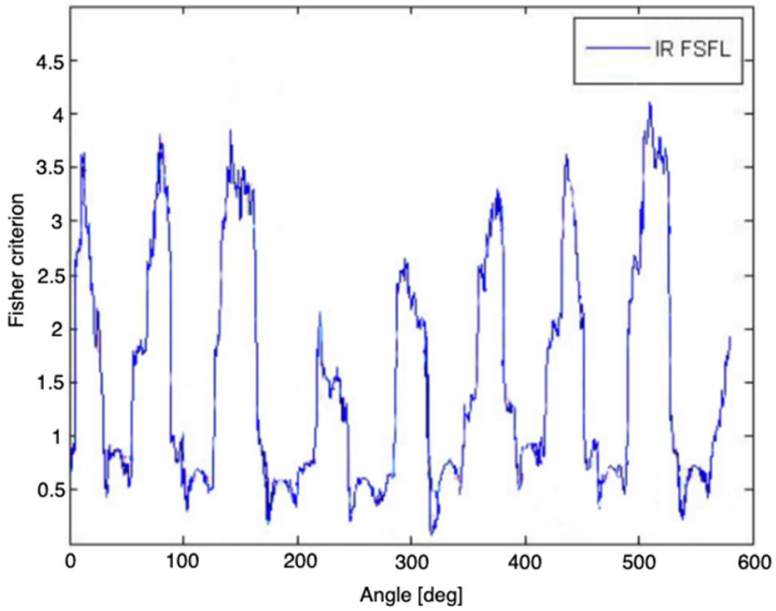

Figure 8. The FC measures of diagnostic feature separation between inner race defect and undamaged case.

Table 3. Comparison of FC for the wavelet approach [5] and the proposed approach.

Rolling Element N	Wavelet	SK	Gain
1	1.2	3.6	3
2	1.2	3.8	3.2
3	1.1	3.9	3.5
4	1.1	2.1	1.9
5	0.9	2.6	2.9
6	1.2	3.3	2.8
7	1	3.6	3.6
8	0.9	4.1	4.6

Hence, according to the higher FC values in Table 3, the proposed technology offers much better separation and superior diagnostics compared to the wavelet approach. The diagnostic features, extracted via the proposed technology indicate FC values with a mean of 3.4 (Figure 8). The results indicate effectiveness gain (EG) in range of [1.9, 4.6] in terms of the FC, where EG is the ratio of the FC of the proposed technology to the FC of the wavelet technology $EG = \frac{FC_{SK}}{FC_W}$.

The experimental validation of the proposed technology is also estimated via artificial intelligence decision making, using the k-NN and k-means supervised approaches. Upon creating the clusters, representing undamaged conditions, using the k-means technique and training data from fault-free case, the testing diagnostic features from undamaged and damaged cases were classified. As a result, the decision maps in Figure 9 shows the amount of false detections and missed detections.

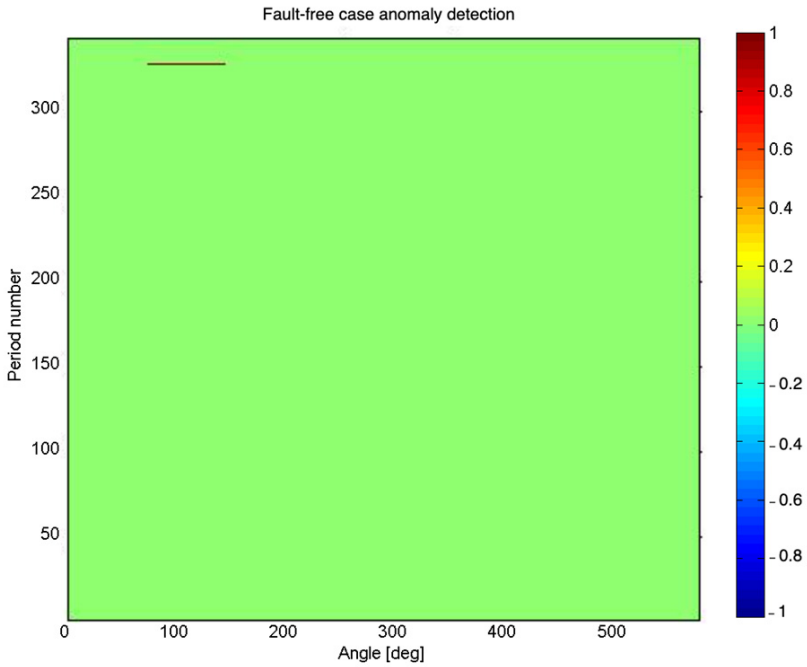

(**a**) Fault-free

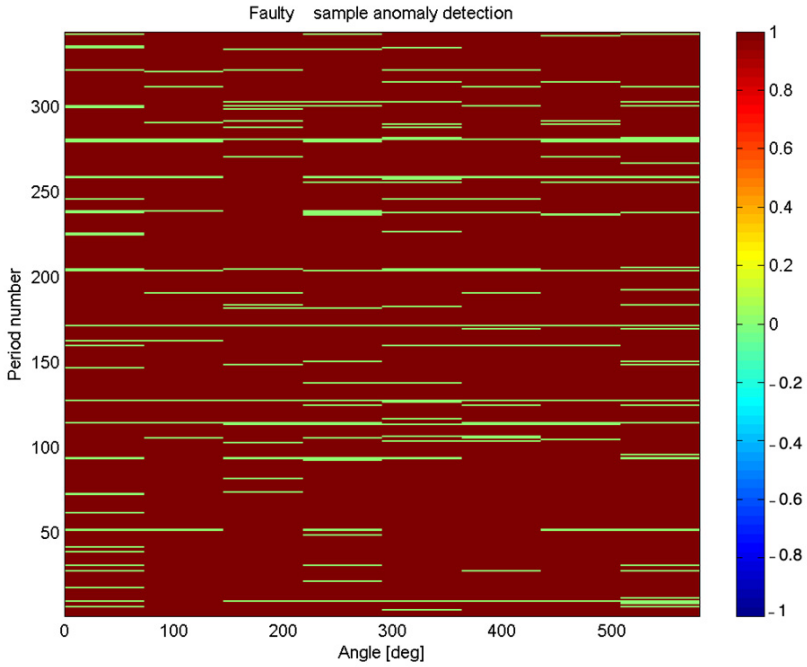

(**b**) Damaged

Figure 9. The anomaly detection decision maps, obtained using k-means and k-NN approaches for bearing signal.

In the undamaged case (Figure 9a), the number of false alarms is relatively low, equal to 0.1%. In the damaged case (Figure 9b), the number of missed detections is 7.7%. The total probability of correct diagnosis (TPCD) equals to 96.2%, which can be considered as a successful diagnosis.

4. Technology Validation Via Simulation for Fault Diagnosis of Gear Pitting

The mathematical model, used to simulate gear vibrations under undamaged and damaged conditions is a lumped mass model, which considers spur gears as rigid disks, coupled along the line of action through a time varying mesh stiffness, as shown in Figure 10 [31].

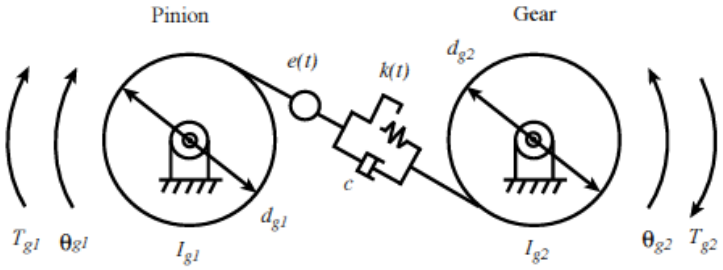

Figure 10. Dynamic model of spur gear pair [31].

Number of teeth is equal to 31 for a pinion and 39 for a gear. Vibration data for each case are sampled using a sampling frequency of 80 kHz and provided recordings of 25 s duration. The speed of the gear shaft is equal to 307.7 rpm (5.1 Hz).

Two sets of simulations were performed: the first set contained no tooth damage, and the second set contained 15% relative pitting size, which is a ratio between the damaged and total tooth areas; pitting is distributed equally among all 39 teeth. The pitting level is simulated by reducing the tooth meshing stiffness.

Authors in [31] have developed an accurate rotation speed estimation method from the gear mesh harmonics appearing in the vibration signal. To extract the instantaneous speed, a narrow-band filter is centered at the mesh frequency.

The instantaneous speed profiles are used for angular resampling procedure to transform vibration signals from time into the angular domain. The angular resampled vibration signals were time-synchronous averaged to isolate vibrations, related to a single gear, from another mechanical component. The main parameter of the TSA is the number of rotational segments to be averaged, which is defined via minimization of the TSA variance. For this purpose, a TSA convergence analysis is performed, which revealed a reliable TSA estimate, based on 20 segments. From the entire vibration signal a total of 127 shaft rotation segments were obtained. Since the TSA is calculated from 20 consecutive segments and s performed without overlapping, a total of 6 TSA signals were obtained for further analysis.

The spectral kurtosis (SK) is estimated for 6 consequent segments of the gear residual signal obtained after removing mesh harmonics from the TSA signal. Figure 11 shows SK segments for (a) fault-free and (b) damaged cases, which is estimated using a Hamming window of size equal to half mesh period. In the damaged case, the SK shows values above 3 within the frequency band of 0 Hz to 6 kHz compared to undamaged case, which are related to the resonant frequencies of the structure and should therefore be considered for filtering. It is also evident, that in the fault-free case, the SK acquired values above 0.5 within 0 Hz to 9 kHz, which indicates weak non-stationary behavior even in the case of no damage.

The SK threshold for filtering is set to 1. Figure 12 shows the diagnostic features for all 39 teeth and 6 segments. The feature values for the damaged case (b) are significantly higher compared to the features from undamaged case (a) and have a mean feature value equal to 6.2×10^{-3} compared to the undamaged case mean feature value of 10^{-6}. Several orders of magnitude higher feature values confirm good separation between the undamaged and damaged cases.

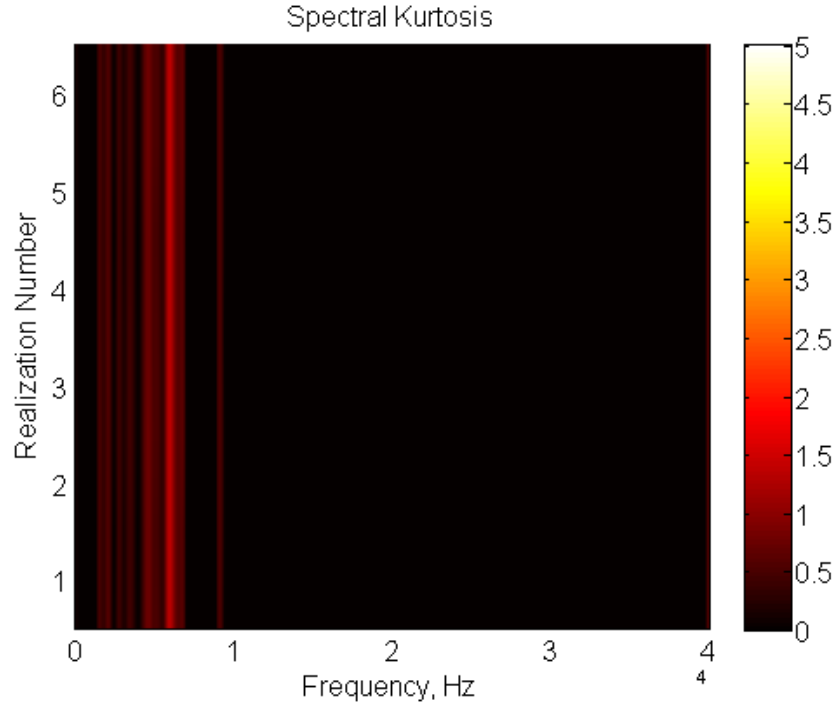

(**a**) No defect

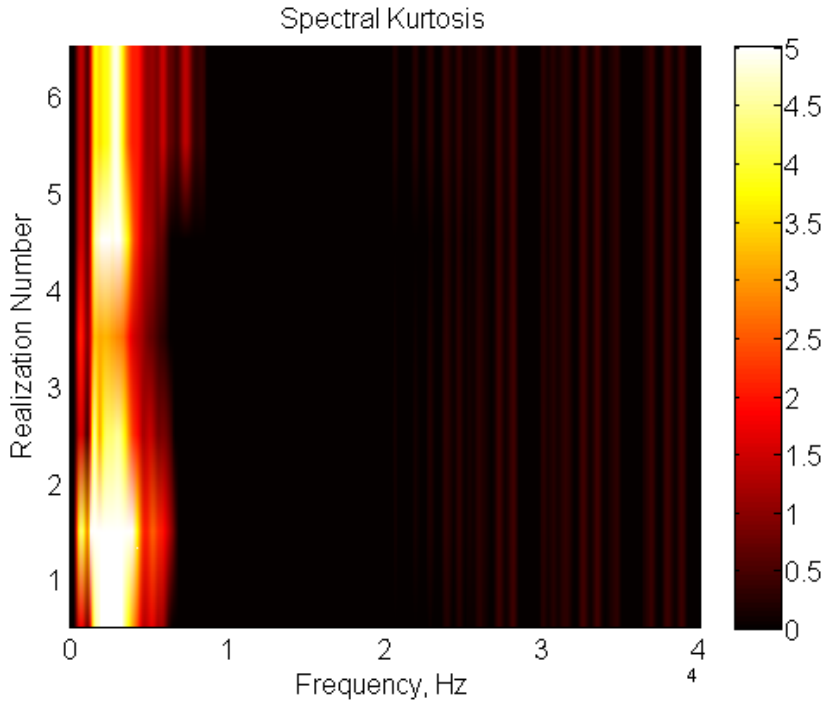

(**b**) Gear pitting defect

Figure 11. Spectral kurtosis for consequent gear vibration segments.

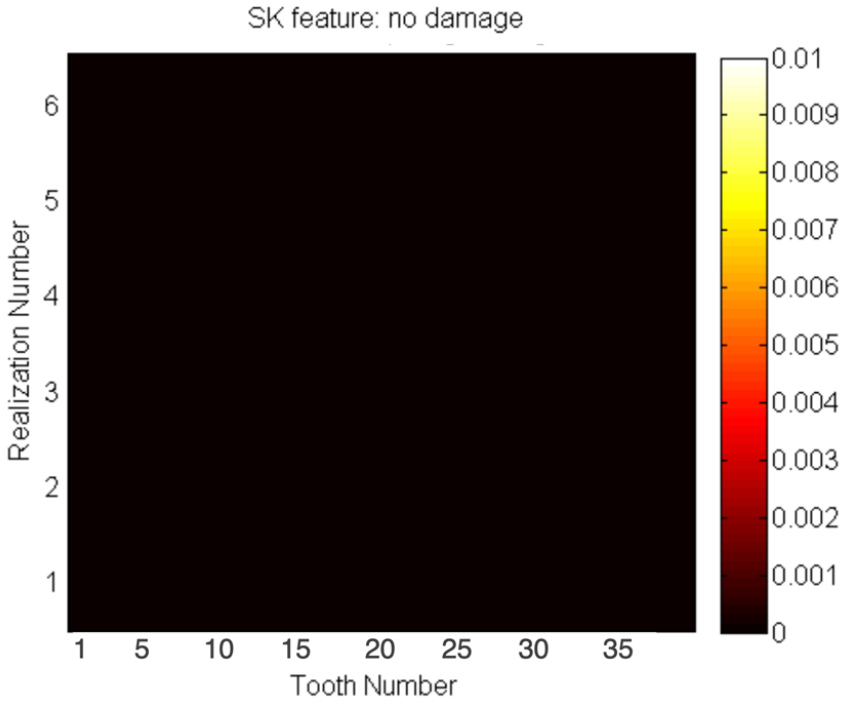

(**a**) No defect

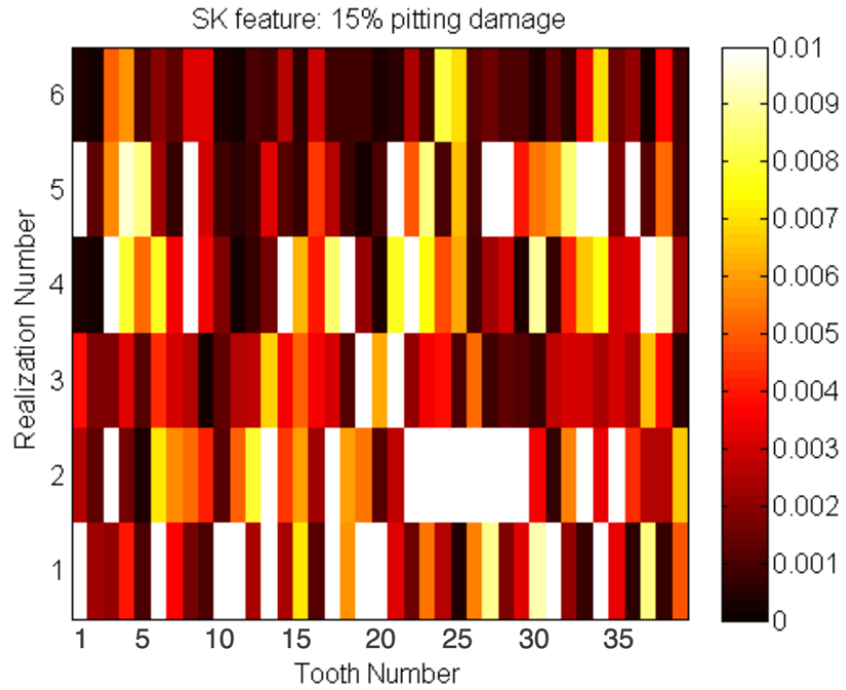

(**b**) Gear pitting defect

Figure 12. The diagnostic features—squared envelope of the filtered SK-residuals from gear signal.

Figure 13 shows the FC independently for each of the 39 teeth for the selected SK window durations and thresholds for filtering. Different filtering thresholds and window sizes were also used for comparison purposes. The FC for half-mesh period and filtering threshold equal to 1 shows very similar results for the other cases, where the FC acquired values above 0.5 with a maximum peak value equal to 6. The only case, which shows poorer separation among diagnostic features is the case where half mesh period is used in

combination with a threshold 3. In this case, the FC values mostly remain below 0.5. The reason for a poor performance with half mesh period and 3 SK threshold is related to a SK threshold: if a threshold being set too high, potentially above SK amplitude values for a damaged case, then the estimated frequency bands based on the SK values remaining above the threshold will be narrow and reduce to zero when the threshold and SK peak values are the same.

Figure 14 shows results obtained by kNN classification of the diagnostic features, extracted using the SK window of half mesh period and filtering threshold of 1. For supervised training, a set of diagnostic features, extracted from the fault-free case is used for k-means clustering. Overall, the fault diagnosis results in full separation between diagnostic features from undamaged and damaged conditions amounting to 0% missed detection, 0% false alarms and 100% of the probability of the correct diagnosis. This result is obtained using 234 diagnostic features for the undamaged case and 234 diagnostic features for the damaged case.

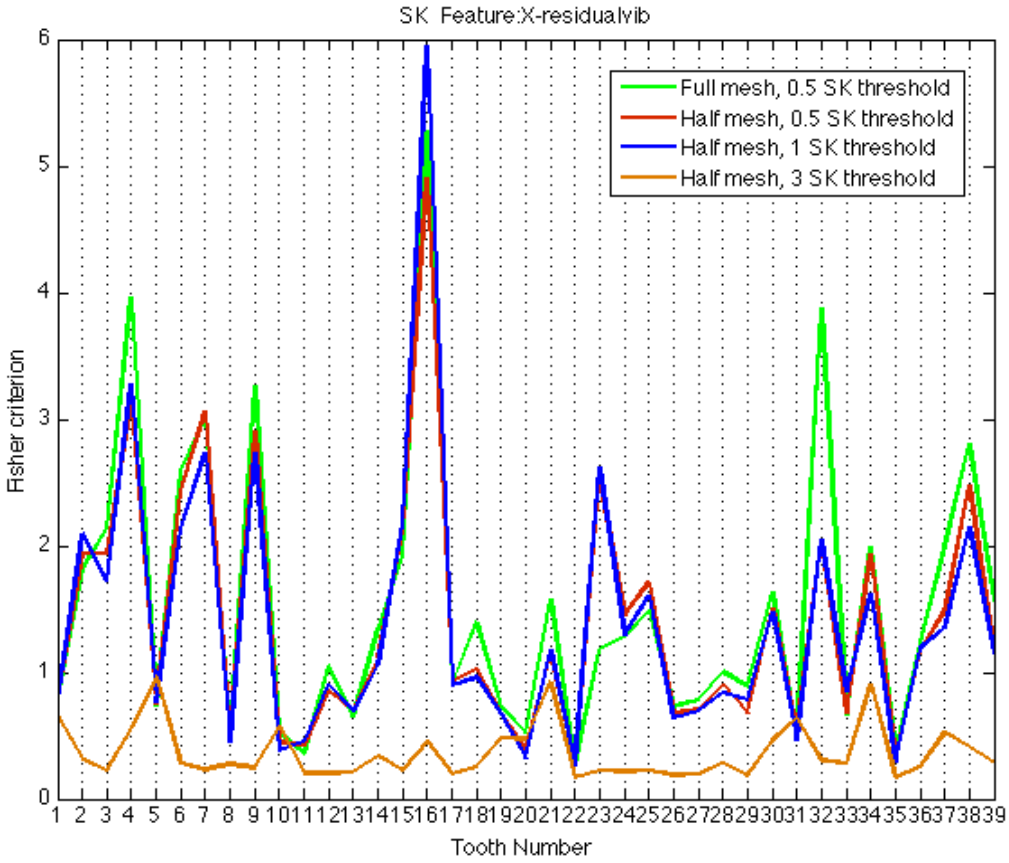

Figure 13. The FC for each tooth and combinations of SK window sizes and thresholds for SK based filtering.

While the estimate of the high probability of correct diagnosis of 100% is achieved, it is important to note, that the results are based on early-stage damage levels of 15%, distributed across all teeth. This suggests that more simulated work and experimental work are needed to validate the approach for a very early stage tooth damage development.

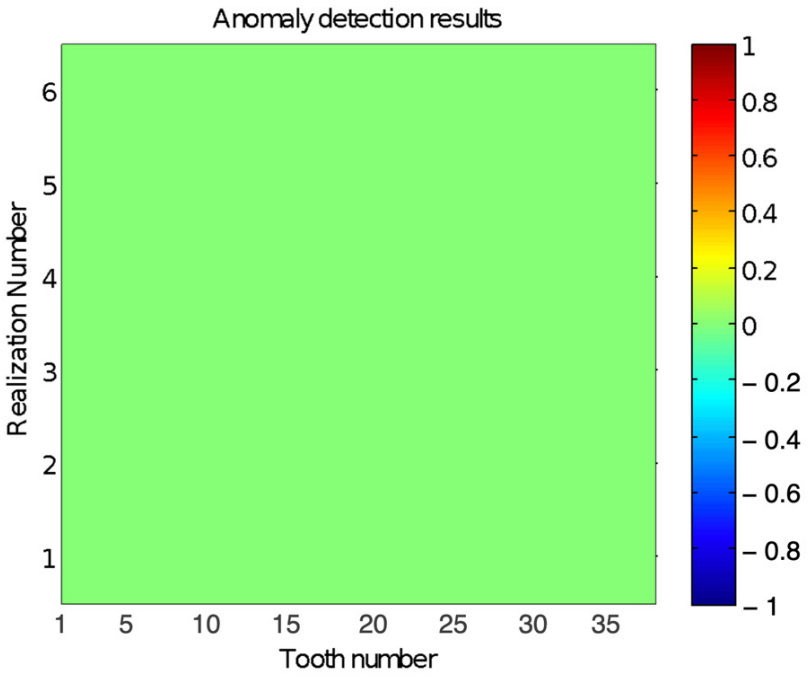

(**a**) Fault-free

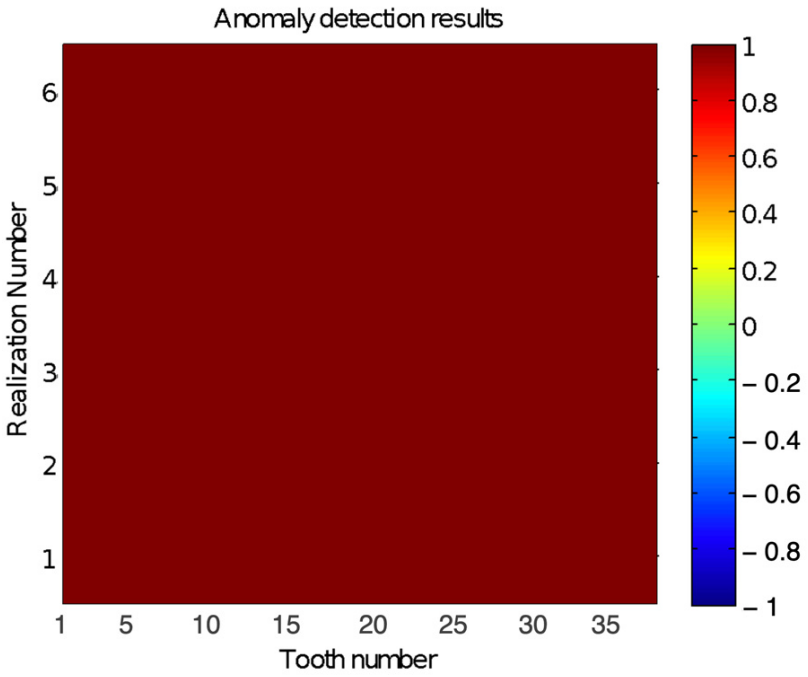

(**b**) Damaged

Figure 14. The anomaly detection decision maps, obtained using k-means and k-NN approaches for gear signal.

5. Conclusions

The novel diagnosis technology, based on the simultaneous processing of multiple spectral kurtoses (SK) and SK based optimal denoising Wiener filtering, is proposed, experimentally validated for early diagnosis of local damage of rolling element bearings and validated via simulation for diagnosis of a gearbox under undamaged and pitted conditions.

The main novelty of the proposed technology is division of bearing/gear vibration signals into specially defined short duration segments and simultaneous analysis/processing of SKs of all these segments for damage diagnosis. The SK is used to identify the frequency bands of the fault related impulses in short vibration segments. The approach tackles diagnostic challenges due to bearing slippage using cross-correlation technique to track impulsive responses, caused by rolling elements that are going over a damaged area.

The experimental technology validation is performed on early diagnosis of a bearing inner race defect (1.2% relative damage size). The separation of histograms of the diagnostic features for fault-free and damaged cases is measured by the FC, which shows essential separation with FC values between 2.5 and 4.5. The proposed technology provides successful diagnosis results, with 96.2% estimate of the total probability of the correct diagnosis, 0.1% of false alarms and 7.7% of missed detections.

The diagnostic effectiveness, of the proposed approach is shown to be superior to the wavelet diagnosis approach. While the wavelet approach achieved feature separation with a mean FC of 1.1, the proposed approach achieved feature separation with a mean FC of 3.4 and an effectiveness gain in range of [1.9, 4.6] in terms of the FC.

In the case of gears, processing of the simulated data revealed very good separation between diagnostic features from undamaged and damaged conditions with the FC reaching up to 6 for some of the teeth. and 100% estimate of the total probability of the correct diagnosis.

The use of SK for bearing/gearbox diagnosis via simultaneous processing of SKs of specially defined short vibration segments makes the technology efficient, adaptive, and easily implementable for on-line industrial applications. Alternatively, as shown in [22,32–35], the SK can be used as a pre-processing technique for wavelet-based diagnosis, thus, offering a possibility of a fault diagnosis via combining several techniques.

A continuation of work towards an ablation study, which would further evaluate the method's effectiveness, would be focused on gears for which we are planning experimental testing with a very early stage of a damage. For bearings we do not see a need for reducing the bearing damage size given that the current data contains a very early stage of a bearing damage.

Author Contributions: Conceptualization, L.G.; methodology, L.G. and G.P.; software, G.P.; validation, L.G. and G.P.; formal analysis, L.G. and G.P.; investigation, L.G. and G.P.; writing—original draft preparation, G.P.; writing—review and editing, L.G.; visualization, G.P.; supervision, L.G. All authors have read and agreed to the published version of the manuscript.

Funding: This research received no external funding.

Institutional Review Board Statement: Not applicable.

Informed Consent Statement: Not applicable.

Data Availability Statement: Not applicable.

Acknowledgments: The authors would like to express special thanks to SKF for the support, T. Patel for performing experimental trials, F. Pellicano and M. Barbieri for supplying gear simulated data and A. D. Ball (the University of Huddersfield) for valuable comments and manuscript review.

Conflicts of Interest: The authors declare no conflict of interest.

References

1. McFadden, P.D.; Smith, J.D. Vibration monitoring of rolling element bearings by the high-frequency resonance technique—A review. *Tribol. Int.* **1984**, *17*, 3–10. [CrossRef]
2. Tandon, N.; Choudhury, A. A review of vibration and acoustic measurement methods for the detection of defects in rolling element bearings. *Tribol. Int.* **1999**, *32*, 469–480. [CrossRef]
3. Randall, R.B.; Antoni, J. Rolling element bearing diagnostics—A tutorial. *Mech. Syst. Signal Process.* **2011**, *25*, 485–520. [CrossRef]
4. Gelman, L.; Kolbe, S.; Shaw, B.; Vaidhianathasamy, M. Novel adaptation of the spectral kurtosis for vibration diagnosis of gearboxes in non-stationary conditions. *Insight-Non-Destr. Test. Cond. Monit.* **2017**, *59*, 434–439. [CrossRef]

5. Gelman, L.; Murray, B.; Patel, T.H.; Thomson, A. Novel wavelet technology for vibration condition monitoring of rolling element bearings. *Insight-Non-Destr. Test. Cond. Monit.* **2015**, *57*, 40–47. [CrossRef]
6. Osman, S.; Wang, W. A leakage-free resonance sparse decomposition technique for bearing fault detection in gearboxes. *Meas. Sci. Technol.* **2018**, *29*, 035004. [CrossRef]
7. Gelman, L.; Soliński, K.; Ball, A. Novel higher-order spectral cross-correlation technologies for vibration sensor-based diagnosis of gearboxes. *Sensors* **2020**, *20*, 5131. [CrossRef]
8. Gelman, L.; Soliński, K.; Ball, A. Novel instantaneous wavelet bicoherence for vibration fault detection in gear systems. *Energies* **2021**, *14*, 6811. [CrossRef]
9. Zhao, D.; Gelman, L.; Chu, F.; Ball, A. Novel method for vibration sensor-based instantaneous defect frequency estimation for rolling bearings under non-stationary conditions. *Sensors* **2020**, *20*, 5201. [CrossRef] [PubMed]
10. Gelman, L.; Murray, B.; Patel, T.H.; Thomson, A. Novel decision-making technique for damage diagnosis. *Insight-Non-Destr. Test. Cond. Monit.* **2013**, *55*, 428–432. [CrossRef]
11. Combet, F.; Gelman, L.; Anuzis, P.; Slater, R. Vibration detection of local gear damage by advanced demodulation and residual techniques. *Proc. Inst. Mech. Eng. Part G J. Aerosp. Eng.* **2009**, *223*, 507–514.
12. Antoni, J.; Randall, R.B. The spectral kurtosis: Application to the vibratory surveillance and diagnostics of rotating machines. *Mech. Syst. Signal Process.* **2006**, *20*, 308–331. [CrossRef]
13. Antoni, J. The spectral kurtosis: A useful tool for characterizing non-stationary signals. *Mech. Syst. Signal Process.* **2006**, *20*, 282–307. [CrossRef]
14. Antoni, J. Fast computation of the kurtogram for the detection of transient faults. *Mech. Syst. Signal Process.* **2007**, *21*, 108–124. [CrossRef]
15. Antoni, J. Blind separation of vibration components: Principles and demonstrations. *Mech. Syst. Signal Process.* **2005**, *19*, 1166–1180. [CrossRef]
16. Sawalhi, N.; Randall, R.B.; Endo, H. The enhancement of fault detection and diagnosis in rolling element bearings using minimum entropy deconvolution combined with spectral kurtosis. *Mech. Syst. Signal Process.* **2007**, *21*, 2616–2633. [CrossRef]
17. Guo, W.; Tse, P.W.; Djordjevich, A. Faulty bearing signal recovery from large noise using a hybrid method based on spectral kurtosis and ensemble empirical mode decomposition. *Measurement* **2012**, *45*, 1308–1322. [CrossRef]
18. Wang, Y.; Liang, M. Identification of multiple transient faults based on the adaptive spectral kurtosis method. *J. Sound Vib.* **2012**, *331*, 470–486. [CrossRef]
19. Persin, G. Fault Detection and Localization of Mechanical Drives Based on Data Fusion Techniques. Ph.D. Dissertation, University of Ljubljana, Faculty of Mechanical Engineering, Ljubljana, Slovenia, 2013.
20. Combet, F.; Gelman, L. Optimal filtering of gear signals for early damage detection based on the spectral kurtosis. *Mech. Syst. Signal Process.* **2009**, *23*, 652–668. [CrossRef]
21. Gelman, L.; Chandra, N.H.; Kurosz, R.; Pellicano, F.; Barbieri, M.; Zippo, A. Novel spectral kurtosis technology for adaptive vibration condition monitoring of multi-stage gearboxes. *Insight-Non-Destr. Test. Cond. Monit.* **2016**, *58*, 409–416. [CrossRef]
22. Kolbe, S.; Gelman, L.; Ball, A. Novel prediction of diagnosis effectiveness for adaptation of the spectral kurtosis technology to varying operating conditions. *Sensors* **2021**, *21*, 6913. [CrossRef] [PubMed]
23. Zhang, Y.; Randall, R.B. Rolling element bearing fault diagnosis based on the combination of genetic algorithms and fast kurtogram. *Mech. Syst. Signal Process.* **2009**, *23*, 1509–1517. [CrossRef]
24. McFadden, P.D. Interpolation techniques for time domain averaging of gear vibration. *Mech. Syst. Signal Process.* **1989**, *3*, 87–97. [CrossRef]
25. Villa, L.F.; Reñones, A.; Perán, J.R.; De Miguel, L.J. Angular resampling for vibration analysis in wind turbines under non-linear speed fluctuation. *Mech. Syst. Signal Process.* **2011**, *25*, 2157–2168. [CrossRef]
26. Stewart, R.M. *Some Useful Data Analysis Techniques for Gearbox Diagnostics*; University of Southampton: Southampton, UK, 1997; MHM/R/10/77.
27. McFadden, P.D. Examination of a technique for the early detection of failure in gears by signal processing of the time domain average of the meshing vibration. *Mech. Syst. Signal Process.* **1987**, *1*, 173–183. [CrossRef]
28. Li, S.Z.; Jain, A. *Fisher Criterion, Encyclopedia of Biometrics*; Springer: Berlin/Heidelberg, Germany, 2009.
29. Boashash, B. Estimating and interpreting the instantaneous frequency of a signal, I. Fundamentals. *Proc. IEEE* **1992**, *80*, 520–538. [CrossRef]
30. Gelman, L.; Petrunin, I. Novel anomaly detection technique based on the nearest neighbour and sequential methods. *Insight-Non-Destr. Test. Cond. Monit.* **2012**, *54*, 433–435. [CrossRef]
31. Barbieri, M.; Scagliarini, G.; Bonori, G.; Pellicano, F.; Bertccchi, G. Optimization methods for spur gear dynamics. In Proceedings of the EUROMECH Nonlinear Dynamics Conference, Saint Petersburg, Russia, 30 June–4 July 2008; pp. 1–6.
32. Combet, F.; Gelman, L. An automated methodology for performing time synchronous averaging of a gearbox signal without speed sensor. *Mech. Syst. Signal Process.* **2007**, *21*, 2590–2606. [CrossRef]
33. Gelman, L.; Patel, T. Novel rolling bearing diagnosis technology using spectral kurtosis and the wavelet higher-order spectra. *Insight-Non-Destr. Test. Cond. Monit.* **2015**, *57*, 452–456. [CrossRef]
34. Gelman, L.; Murray, B.; Patel, T.H.; Thomson, A. Vibration diagnostics of rolling bearings by novel nonlinear non-stationary wavelet bicoherence technology. *Eng. Struct.* **2014**, *80*, 514–520. [CrossRef]

35. Gelman, L.; Patel, T.H.; Persin, G.; Murray, B.; Thomson, A. Novel technology based on the spectral kurtosis and wavelet transform for rolling bearing diagnosis. *Int. J. Progn. Health Manag.* **2013**, *4*, 2153–2648. [CrossRef]
36. Mosleh, A.; Montenegro, A.; Costa, P.A.; Calcada, R. Railway Vehicle Flat Detection with Multiple Records Using Spectral Kurtosis Analysis. *Appl. Sci.* **2021**, *11*, 4002. [CrossRef]
37. Paolo, A.D.; Luigi, G.; Alessandro, F.; Stefano, M. Performance of Envelope and Traditional Indicators vs. Targeted a Posteriori Band Indicators. *Appl. Sci.* **2021**, *11*, 6262. [CrossRef]